Structure of an Evolving Hailstorm, Part III: Internal Structure from Doppler Radar

R. G. STRAUCH AND F. H. MERREM

NOAA/ERL/Wave Propagation Laboratory,[1] Boulder, Colo. 80303

(Manuscript received 17 September 1975, in revised form 12 December 1975)

ABSTRACT

Two X-band Doppler radars observed a hailstorm that passed directly over one of the radars during the 1973 National Hail Research Experiment (NHRE). While one of the radars scanned the storm at low elevation angles the other radar, which operated simultaneously in a zenith-pointing mode, measured part of an updraft. Observations by other NHRE participants assisted in interpreting the radial velocity fields so that inflow and outflow could be identified from the scanning radar measurements. The peak updrafts occurred just ahead of the highest reflectivity while the strongest downdrafts were found only 6 km behind the updraft. Strong turbulence was generated in the transition region between updraft and downdraft as evidenced by large velocity variances. A substantial part of the downdraft appeared to have been fed by air that had ascended in the updraft. Low-level velocity fields were in general agreement with surface measurements and showed the outflow toward the front of the storm in the gust front as well as outflow opposite the echo motion behind the storm. There was strong outflow opposite the direction of echo motion at the top of the storm which agreed with photographs of the anvil overhang.

1. Introduction

The observations discussed in this paper were made with two X-band Doppler radars on a storm that passed directly over one of the radars near Raymer during the 1973 field program of the National Hail Research Experiment (NHRE) in northeast Colorado. The two radars normally were operated as a dual-Doppler system to acquire data for analysis of three-dimensional wind fields. However, when a storm passed directly over one radar, it was operated in a zenith-pointing mode while the second radar scanned an azimuth sector encompassing the zenith-pointing radar with a raster scan stepped in elevation. Browning *et al.* (1968) conducted a similar experiment to observe the horizontal and vertical air motion in a shower, except their second radar scanned in elevation at a single fixed azimuth. The operational mode we selected enabled us to determine the two-dimensional velocity in a vertical plane through the radars, and it also allowed us to observe the reflectivity and one component of air motion throughout the storm volume. Several storms were observed in this operating mode, but the Raymer storm of 9 July 1973 discussed here combines two fortuitous factors in addition to the extensive measurements obtained with other instruments:

1) The storm track was within 5° of the line joining the radars. Thus, inflow and outflow parallel to the direction of storm motion were observed as radial velocity. These regions were clearly seen by the scanning radar and assisted in interpreting the measured radial velocity field in terms of the storm structure.

2) An updraft region passed directly over the zenith-pointing radar. The vertical velocity data could therefore be used to locate the updraft precisely in relation to the storm echo.

2. Doppler radar observations

The location of Doppler radars A and B relative to the NHRE operational area is shown in Fig. 1. The radars were separated by 52.2 km with a baseline angle of 354° from north. The 9 July 1973 hailstorm passed directly over the southern radar (Radar A). Fig. 1 also shows the reflectivity contours, just below cloud base, measured by the NHRE 10 cm radar located at Grover, Colo., at the time the storm was over Radar A. Radar A acquired data in a zenith-pointed mode from 1725:55 to 1736:15 MDT. During this same time, Radar B was scanning an azimuth sector at elevation angles of 0° to 15° in 1° steps. The 16 elevation steps were scanned in 160 s. The area covered by Radar B during its initial scan sequence is outlined by the dashed lines. A representative echo motion was 7 m s^{-1} along the radar baseline during the time interval of interest for the Doppler data. Seven meters per second is an intermediate value between the motion of the storm as a whole and the motion of individual cells (Part I). The dotted line in Fig. 1 shows the coverage of the zenith-pointing radar as the storm advected overhead. The Doppler radar observations pertain to cell W4.

[1] This research was performed as part of the National Hail Research Experiment, managed by the National Center for Atmospheric Research and sponsored by the Weather Modification Program, Research Applications Directorate, National Science Foundation.

The characteristics of the X-band Doppler radars have been described by Frisch *et al.* (1974), but will be briefly summarized here. The complex video signals were digitally recorded for postanalysis. The zenith-pointing radar acquired data at 24 fixed heights with a dwell time of 0.065 s corresponding to 128 radar samples in each height increment. From these data the complete Doppler velocity spectrum was obtainable 96 times per minute at each height. The radar beamwidth of 0.9° provided a horizontal resolution better than 250 m at the maximum altitude. The height resolution was 75 m and the minimum height that could be observed was 1.8 km (MSL). (The radar altitudes were 1.5 km MSL.) The height spacing between data locations was 600 m, with the lowest location centered at 1.9 km and the highest at 15.7 km during the period 1725:55 to 1728:05. From 1728:05 to 1736:15 the height spacing was 300 m with the lowest location centered at 1.9 km and the highest at 8.8 km.

The scanning radar used the same dwell time (0.065 s for 128 radar samples) and acquired data for 384 (16 azimuth × 24 range) radar resolution elements in 10 sec for each fixed elevation step. Four complete elevation scan sequences were made during the 12 min observation period. The 0.9° beamwidth resulted in a spatial resolution of 600 to 800 m at the location of the storm. The data locations were separated by 600 m in range and about 1.5° (1300 m) in azimuth. The entire Doppler velocity spectrum was calculable for each measurement point of the scanning radar so the radial velocity, velocity variance, and radar reflectivity were estimated at each data point.

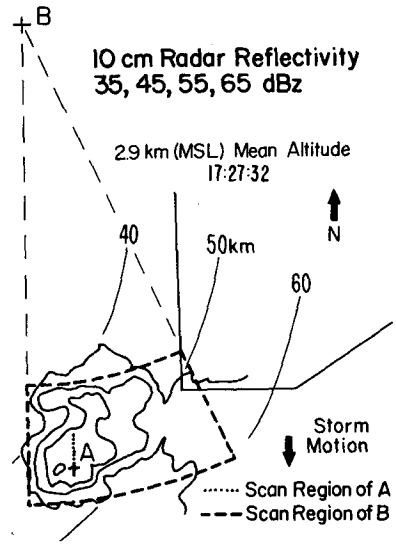

FIG. 1. PPI presentation of NHRE 10 cm radar reflectivity contours near cloud base at 1727 MDT and scan regions for the Doppler radars.

3. Data analysis procedure

The radar reflectivity and the first and second moments of the velocity spectra were estimated from the 128 radar samples recorded at each range location. A fast Fourier transform algorithm was used with a general purpose computer to calculate the Doppler velocity spectra. Each radar acquired data for approximately 28,000 velocity spectra during the 12 min observation period, so that estimates of the spectral moments of the signal had to be made by a high speed computer from the Doppler signal plus noise data. The spectra were estimated from the 128 radar samples and the moments were computed after a velocity window was applied to the spectra. The velocity window ranged on both sides of the peak of the spectrum to points where the power density fell to within 3 dB of the receiver noise level. The windowed spectra were manually checked to ensure that the automated method selected the correct signal spectra and properly accounted for velocity folding. The first and second moments of the velocity spectra were also estimated with a "pulse-pair" algorithm (Berger and Groginsky, 1973). The radar reflectivity factor Z was also calculated from the signal power estimates. The radar reflectivity values were not corrected for attenuation and are, therefore, only approximate. The vertical air motion, W, was estimated by subtracting the terminal fall speed of the particles, V_T, from the measured, reflectivity-weighted particle velocity, V_z. The terminal fall speed of the particles was estimated using the empirical relation $V_T = 2.6\,Z^{0.107}$ of Joss and Waldvogel (1970) as suggested by Atlas *et al.* (1973), with a correction for air density variations proposed by Foote and du Toit (1969). Since the V_T vs Z relationship is relatively insensitive to Z, the estimate of V_T should be accurate to within ± 1 m s^{-1} in rain. The Joss-Waldvogel empirical equation underestimates the fall speed if hail is present in the pulse volume; consequently the updraft would be underestimated.

The reflectivity factor, mean radial velocity, and velocity variance measured by the scanning radar were interpolated into a Cartesian coordinate system with the y axis along the radar baseline. The various quantities were then contoured and displayed in horizontal and vertical planes. Interpolation smoothed out large gradients because adjacent measurement points were used to calculate values on a Cartesian grid. Consequently, examination of the original measurements indicated that maximum gradients of the various quantities were reduced by a factor of about 2 after interpolation. The radial velocity sign convention is such that motion away from the radar is registered as positive. The vertical motion of the particles, V_z, contributes a radial velocity component of magnitude $V_z \sin\theta$ to the velocity measured by the scanning radar, where θ is the elevation angle of the radar antenna. This contribution was always less than 1.5 m s^{-1} in this experiment and was not removed from the radial velocity fields except in the vertical plane containing both

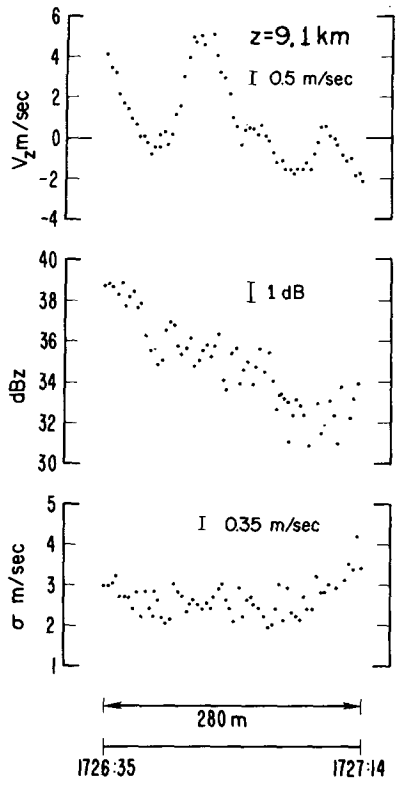

FIG. 2. Forty-second sample of data measured by the zenith-pointing radar. Vertical velocity of the scattering particles of +5 m s^{-1} indicate updraft in excess of 13 m s^{-1}. Bars denote predicted standard deviation of the estimates.

radars because it was known only above the zenith-pointing radar.

In the region where both radars acquired data, two-dimensional air motion was calculated by combining the observations of vertical air motion by the zenith-pointing radar with the horizontal air motion along the radar baseline observed by the scanning radar. The horizontal component of motion, V_h, in the vertical plane through the two radars was derived from the measured radial velocity, V_R, using the relationship $V_R = V_z \sin\theta + V_h \cos\theta$. The two-dimensional air motion field was corrected for echo motion by removing a 7 m s^{-1} component from the horizontal velocity.

4. Nature of the data

An example of the data acquired by the zenith-pointing radar is shown in Fig. 2 to illustrate the temporal variability of the vertical structure. Sixty-four data points from a sample obtained in the updraft region over a period of 40 s are shown. The terminal fall speed computed from the Joss-Waldvogel equation varied from 8.2 to 9.4 m s^{-1} for the reflectivity values shown in Fig. 2 (center), so the maximum updraft must have exceeded 13 m s^{-1}. The particle velocity V_z changed 6 m s^{-1} in 8 s with little change in reflectivity, demonstrating that rapid changes can occur in the updraft. The beamwidth was about 120 m at 9.1 km altitude, and the pulse length was about 75 m. The 6 m s^{-1} velocity change, therefore, occurred while the echo was advected about $\frac{1}{2}$ beamwidth. If the velocity change had been caused by horizontal shear within the updraft, a shear of 10^{-1} s^{-1} would have been required. A vertical velocity gradient of 7×10^{-2} s^{-1} in an updraft of 10 m s^{-1} would also account for the velocity change.

Fig. 2 can also be used to estimate the accuracy of the measured data. The standard deviation of the mean particle velocity, V_z, (top trace) is given by Miller and Rochwarger (1970) as

$$\left[\frac{\lambda\sigma}{4T_D}\right]^{\frac{1}{2}},$$

where T_D is the dwell time, λ the radar wavelength (0.0322 m) and σ the width of the velocity spectrum. The dwell time is the pulse repetition period (512 μs) multiplied by the number of pulses making up the sample from each volume increment (128), so $T_D = 0.065$ s. The average width of the spectra (bottom trace) is about 2.5 m s^{-1} so the standard deviation of the mean velocity estimate is about 0.5 m s^{-1}. The reflectivity estimates (center trace) are calculated from 128 radar samples, but the number of independent samples is given by Nathanson (1969, p. 89) as

$$N_I = \frac{4\sqrt{\pi}\sigma T_D}{\lambda}.$$

In this experiment there are about 30 independent samples. The standard deviation of the reflectivity estimates is therefore about 1 dB. The standard deviation of the estimates of spectral width, σ, is given by (Miller and Rochwarger, 1970)

$$\left[\frac{3\lambda\sigma}{32T_D}\right]$$

and is about 0.35 m s^{-1} for the data in the lower trace of Fig. 2.

Fig. 3 shows examples of vertical profiles of vertical particle velocity measured in the 0.065 s dwell time. The spatial samplings are for range gate spacings of 600 m (at 1726:01 MDT) and 300 m (1735:01 and 1730:31). The profile measured at 1726:01 illustrates the vertical variability of the velocity structure, particularly in the updraft region about 6.5 km. At 1730:31 the maximum altitude of the measurements had been reduced from 15.7 to 8.8 km. The profile in the center trace of Fig. 3 indicates a downdraft existed over the radar at that time. The profile measured at 1735:01 in the back portion of the storm shows weak downdrafts. Particle velocities as high as +12 m s^{-1} were measured in the updraft at 1726:01, but 4.5 min later, after the

storm had advected less than 2 km, velocities of −20 m s^{-1} were measured.

5. Results

a. Air motion in the vertical plane through the radar sites

Fig. 4a shows the time vs height plot of the 10 cm radar reflectivity above the zenith-pointing radar. The dotted line outlines the time and height of the data acquired by the zenith-pointing radar. As can be seen in Fig. 4a the operator of the zenith-pointing radar reduced the maximum observed altitude shortly after the upper-level high reflectivity region had passed overhead. Radar B scanned all of the echo structure shown in Fig. 4a except for the very earliest and latest portions.

Fig. 4b shows contours of vertical air motion derived from the Doppler velocities and reflectivity measured by the zenith-pointing radar using the Joss-Waldvogel equation to remove the V_T component. Five-second averages (8 values) of Z and V_z were used to derive an estimate of W every 5 s, or 35 m for an echo motion of 7 m s^{-1}. The time-height values of W represent the region inside the dotted outline of Fig. 4a. No updrafts were observed below 6.5 km, but the trend of the data suggests that the low-level portion of the updraft had advected past Radar A before 1725. The boundary of the surface outflow passed the radar at 1715 while the leading edge of the low-level echo arrived at 1725. Maximum updraft values occurred between 8.0 and 10.3 km altitude. The slope of the updraft contours indicates that the updraft was tilted toward the north—opposite to the direction of echo motion. This tilt was about 20° from the vertical at 9 km altitude. Highest downdrafts were measured between 3 and 5.5 km altitude and occurred just behind the updraft. The back portion of the storm contained weak downdrafts in the lower levels, but near the highest altitude observed there were weak updrafts, even after the portion of the storm with highest reflectivity had advected past.

The two-dimensional air motion in a vertical plane through the storm observed by both radars is shown in Fig. 4c. The vector representation shows the air motion relative to the storm in the region outlined by the dotted lines in Fig. 4a. The transition between strongest updraft and strongest downdraft probably took place over a distance of about 3 km, and as we shall show, strong turbulence was generated in this region. The most intense part of the downdraft appears to have been fed by air which had ascended in the updraft, as postulated by Newton (1963). The peak downdraft occurred in the region of highest reflectivity and water loading probably contributed to the downdraft.

Reflectivity contours measured by Radar B in the vertical plane through the radars are shown in Fig. 5a. The highest reflectivity factors measured by the 3 cm radar were about 50 dBZ and occurred at an altitude of 5.5 km and 2 km west of the baseline joining the

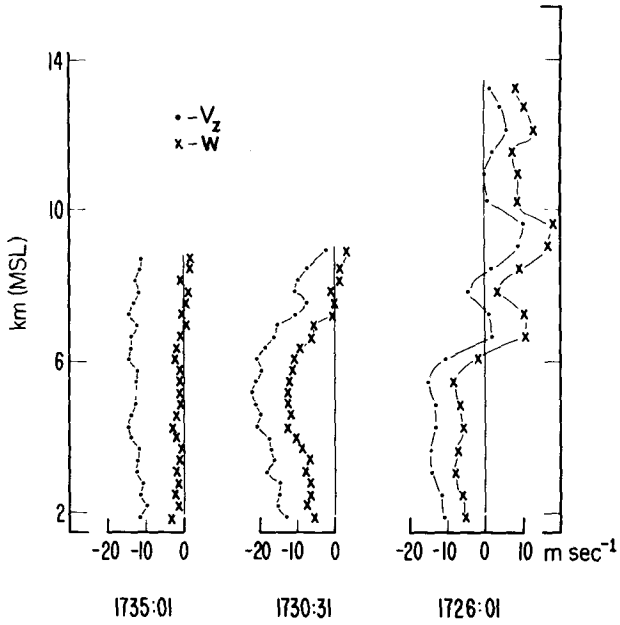

FIG. 3. Vertical particle velocity (V_z) profiles measured by the zenith-pointing radar and vertical wind (W) estimates derived from the Joss-Waldvogel V_T−Z relation.

radars. The 3 cm radar reflectivity contours shown in Fig. 5a are plotted from data acquired between 1727 and 1729:40 while the radar scanned through 16 elevation angles. The time-height plot of 10 cm radar reflectivity factor shown in Fig. 4a is a 30 min history of the reflectivity over Radar A. Reflectivity plotted in Figs. 4a and 5a should have been the same if 1) attenuation of the 3-cm radar was negligible, 2) the storm track was from 354° during the time period 1720 to 1750, 3) the storm was in steady-state during this time, and 4) both radars were properly calibrated. None of these conditions was precisely satisfied. Reflectivity gradients at the leading and trailing edges of the storm appear similar in the two plots, although the measured reflectivity values were greatly different. Attenuation of the 3 cm radar signals would be most noticeable at mid-level of the leading edge of the storm, but the 3 cm radar reflectivity contours portray a structure similar to that depicted by the 10 cm radar.

The radial velocity field (measured by Radar B) shown in Fig. 5b corresponds to the time and location of the reflectivity data shown in Fig. 5a. The velocity contours are absolute velocities; there is no correction for the echo motion and no correction for the terminal fall velocity contribution. Negative velocities are directed toward Radar B and positive velocities are directed away from it. Strong updrafts were measured above Radar A during the time these data were collected by Radar B. The velocity field in Fig. 5b suggests the location of the updraft even without verification from Radar A. Air feeding the updraft entered the storm from the right side of Fig. 5b (Part I). Fig. 5b indicates that the air was moving into the storm at mid-levels

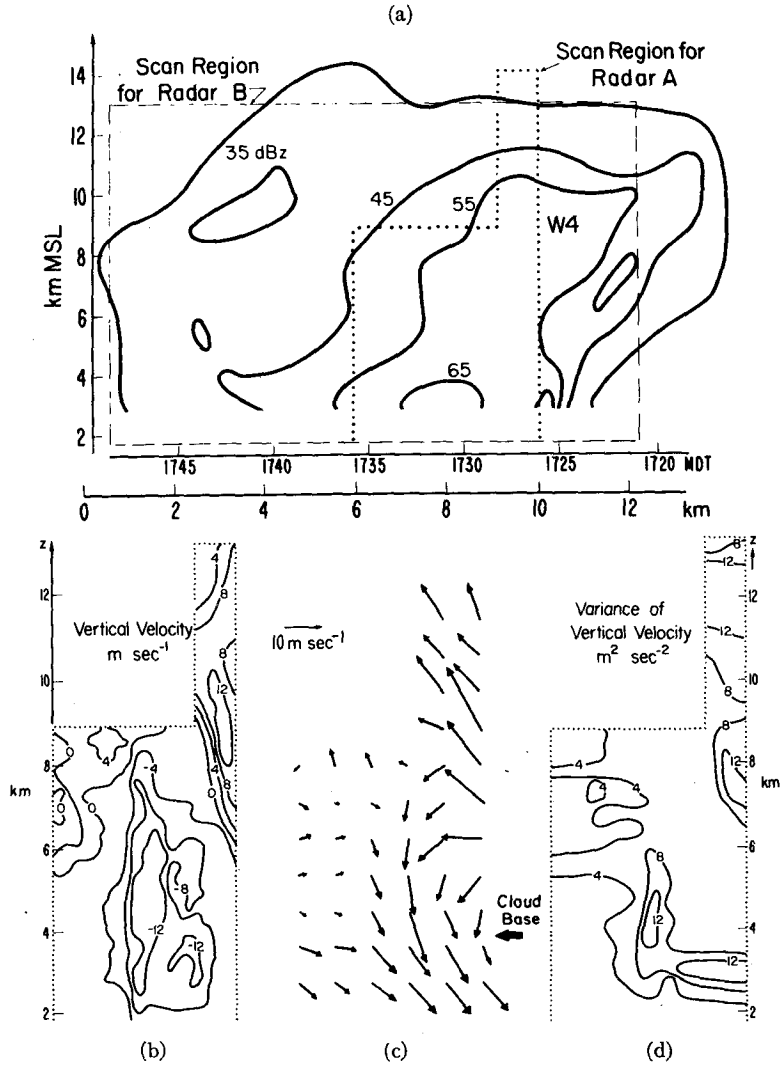

FIG. 4. (a) Time-height presentation of 10 cm reflectivity contours measured over the zenith-pointing Doppler radar and the scan regions for the Doppler radars. (b) Averaged vertical wind contours measured by the zenith-pointing radar from 1726 to 1736 MDT. (c) Two-dimensional air motion relative to the storm echo motion in the vertical plane through the two Doppler radars. (d) Averaged velocity variance measured by the zenith-pointing radar.

with a horizontal velocity component as high as 10 m s^{-1} relative to the storm. The region of high radial velocity gradient above Radar A clearly defines the interface that existed between the updraft and downdraft. The measured component of air flow at the rear of the storm above 7.5 km was generally similar to that in the near environment as measured by the nearest representative radiosonde. Mid-level air was overtaking the storm from the backside at 6.5 to 8.5 km altitude. The outflow at the top of the storm had a strong northward component of more than 15 m sec^{-1} relative to the storm. The trend of the radial velocity in the y direction suggests that weak outflow at the top of the storm could have occurred in the direction of echo motion. It seems unlikely that this implied weak outflow would have been strong enough to have led to particle recirculation to account for the few larger hailstones found in this storm. The velocity field shown in Fig. 5b is in agreement with photographs which show a small anvil overhang in the direction of echo motion (Part II) and a large anvil overhang toward the northeast. The surface anemometer readings of 13 to 17 m s^{-1} are higher than the velocities seen by the radar in the gust front, and they therefore indicate that the strongest low-level outflow in the direction of echo motion occurred in the lowest few hundred meters; this was not observed by the radar.

b. Air motion in horizontal planes

Fig. 6(a)–(c) shows the radial velocity fields measured by Radar B at 3 altitudes. These data were acquired during the time period 1727 to 1729:40. The lowest altitude is labeled 1.8 km, but the antenna pattern at elevation angles corresponding to this altitude was distorted by ground blocking so the data shown for this altitude are actually more representative of the wind field at about 2.1 km. The radial velocity fields in Fig. 6 are not corrected for echo motion. The velocity field at low altitude reveals outflow in the direction opposite the echo motion and also outflow in the gust front. The radial velocity field at 6.5 km (Fig. 6b) shows the strong convergence of the updraft air at the south or leading edge of the storm and the downdraft air from the backside that was overtaking the storm over a wide area. Two regions of air moving into the storm (contours labeled -2 m s^{-1}) probably correspond to the two distinct inflow branches toward W4 and W5 as identified in Part I. The main updraft of W4 had just advected past Radar A at this altitude when these data were acquired. The maximum radial velocity shear indicated by these contours is about 5×10^{-3} s^{-1} whereas the data prior to interpolation indicate peak shear values greater than 10^{-2} s^{-1}. The updraft and downdraft regions of the storm were readily distinguished on the basis of the radial velocity fields measured by Radar B because inflow and outflow parallel to the direction of storm motion was observed as radial velocity. The low and mid-level radar data in Fig. 6 show that the cell that passed over Radar A was contiguous with a line of cells that formed about 30 km to the east.

The radial velocity contours at 11.5 km (Fig. 6c) show the strong divergence near the top of the updraft. Particle velocities at this level appeared as though the particles were ejected from a fountain. The motion relative to the storm was strongly toward the north over a wide area at the back of the storm. The environmental winds at this altitude were from the west-southwest at about 12 m s^{-1}, corresponding to a radial component of only about 3 m s^{-1}. Particle velocity with a southerly component of 4 to 7 m s^{-1}, nearly equal to the echo motion, occurred in front of the updraft at 11.5 km altitude so that some outflow in the direction of echo motion was likely.

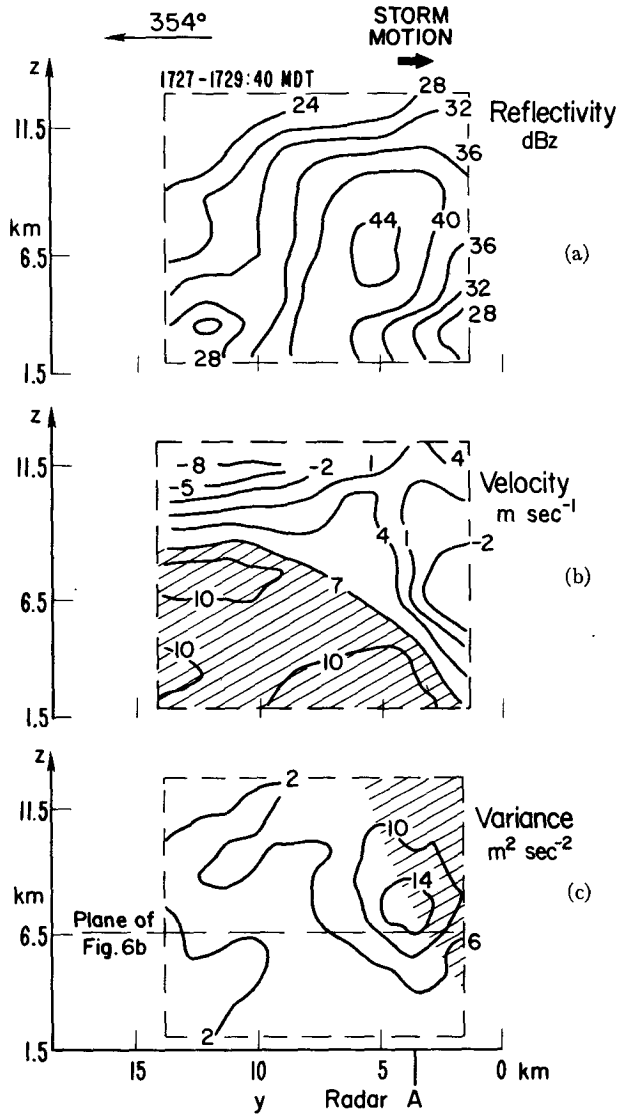

FIG. 5. (a) Three-centimeter radar reflectivity, (b) radial particle velocity, and (c) velocity variance measured by Radar B in the vertical plane through the two Doppler radars. The region inside the dashed lines corresponds to the scan region for Radar B shown in Fig. 4a. The shaded region in b indicates radial velocities that exceed the echo motion of 7 m s^{-1}. The shaded region in (c) indicates where the zenith-pointing radar measured the main updraft. Radar B was located at $y=52.2$ km.

c. Distribution of turbulence inferred from the variance of the velocity

There are three major factors that can contribute to the variance or second moment of the Doppler spectrum measured by a radar with a narrow beamwidth: wind shear, turbulence, and the spread of particle fall speed in still air (Atlas, 1964). The contribution to the variance caused by fall speeds is given by $\sigma_D^2 \sin^2\theta$ where σ_D^2 is the variance that would be observed in still air at vertical incidence. σ_D^2 is about 1 m^2 s^{-2} for rainfall and is nearly independent of rainfall rate (Lhermitte, 1963). For hail with a maximum diameter of 1.5 cm, as occurred in this storm, σ_D^2 is 4 to 6 m^2 s^{-2} (Battan, 1974). The variance caused by wind gradients parallel to the radar beam is given by (Sirmans and Doviak, 1973)

$$\frac{(k_R h)^2}{12}$$

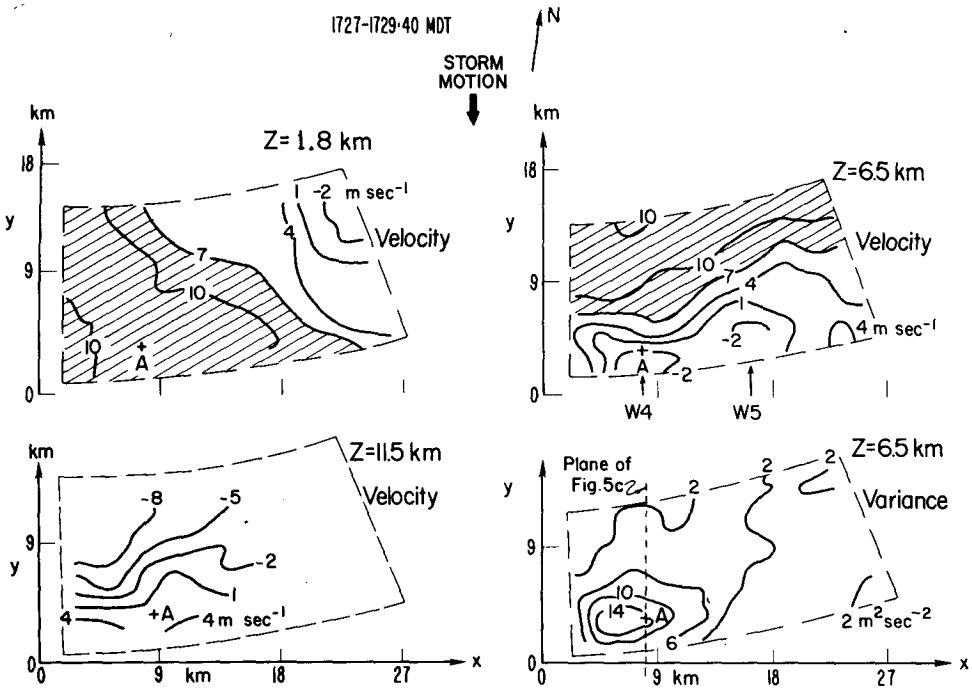

FIG. 6. Radial particle velocity (absolute) at (a) 1.8 km altitude, (b) 6.5 km altitude, and (c) 11.5 km altitude measured by Radar B located 50 km north of the storm. The shaded regions indicate radial velocities that exceed the storm motion of 7 m s^{-1}. (d) Velocity variance at 6.5 km altitude. The scan regions are the same as those shown in Fig. 1.

where k_R is the radial shear (s^{-1}) along the beam and h is the pulse length. For shear across the beam, the variance contribution is given by $(0.3\ k_T\ R\Phi)^2$, where k_T is the radial shear transverse to the beam (Nathanson, 1969, p. 207), R is the range, and Φ is the one-way half-power beamwidth.

All factors that contribute to the variance must be considered for the zenith-pointing radar but the fall speed spread can be neglected for the quasi-horizontally scanning radar because the contribution caused by fall speed was at most 0.08 $m^2\ s^{-2}$ in rain and 0.5 $m^2\ s^{-2}$ in hail. The measured variances in this storm were much greater than 0.5 $m^2\ s^{-2}$ in regions where hail was probably present and much greater than 0.08 throughout the storm. Since the fall speed spread was negligible for the scanning radar and since the radial velocity field was measured throughout the storm, thus making the radial shear known, the turbulence throughout the storm could be calculated from the variance field measured by the scanning radar (Strauch *et al.*, 1975).

The velocity variance measured by Radar A is shown in Fig. 4d and the variance measured by Radar B is shown in Figs. 5c and 6d. Variance data from the zenith-pointing radar were contoured after smoothing by taking an 8-point (5 s) average. High variances were observed by Radar A in two regions of the storm: at mid-levels where Radar B also measured high variances and just below cloud base where Radar B did not measure high variance. The low-level band of high variance must therefore be attributed to spread in particle fall speeds. In fact, shear or turbulence would have caused Radar B to measure larger variances than Radar A because the pulse volume of Radar B was much larger. The large variance at mid-levels seen by Radar A were caused, in part, by shear and turbulence. Fig. 2 shows that its beamwidth was too large to resolve strong local horizontal gradients in the updraft, so this kind of local shear would be interpreted as turbulence in its contribution to the variance. Variances measured by Radar B (Figs. 5c and 6d) at the back of the storm were less than 2 $m^2\ s^{-2}$ and can be attributed to vertical gradients of the radial velocity since the vertical shear of $5\times10^{-3}\ s^{-1}$, seen in Fig. 5b, is sufficient to cause a variance exceeding 2 $m^2\ s^{-2}$. On the other hand, the core of large variance between 5.5 and 9.5 km in Figs. 5c and 6d cannot be attributed to shear because the large shear in this region was parallel to the beam, and its contribution to the variance was small since the pulse length was only 75 m. This region contains large gradients in the vertical velocity (Fig. 4c) but these gradients do not contribute significantly to the variance observed by Radar B. We conclude that the high variance core measured by Radar B was caused mainly by turbulence generated by the large horizontal shear of the vertical wind at the interface between updraft and downdraft. The dissipation rate, ϵ, derived from the velocity variance field measured by Radar B varied from less than 30 $cm^2\ s^{-3}$ at the back of the storm to

more than 3000 cm^2 s^{-3} in the region between the updraft and downdraft (Strauch *et al.*, 1975). These values span the entire range of values measured by aircraft in clear air turbulence.

We assumed that the outer scale in the inertial subrange was larger than the largest dimensions of the radar pulse volume (800 m). Energy spectra with a $-5/3$ power law to scales greater than 1.5 km have been measured with penetration aircraft in thunderstorms (Steiner and Rhyne, 1962). The radial velocity fields shown in Figs. 5b and 6a seem to indicate that the outer scale is no larger than the radar resolution since they do not contain fluctuations at scales of 1 to 2 km. However, the interpolations used to transform the measured data to Cartesian grid points filtered the energy spectrum at scale sizes between the radar beamwidth and the outer scale so the radial velocity fields show only organized motions. Spectra measured with penetration aircraft in severe Oklahoma storms (Steiner and Rhyne, 1962) showed dissipation rates that exceeded those measured by our radar.

6. Conclusions

The Doppler radar measurements described constitute a unique data set because, for the first time, a zenith-pointing radar observed part of the storm as it advected overhead while, at the same time, a scanning Doppler radar obtained the three-dimensional field of reflectivity, radial velocity, and the velocity variance of the radial velocity in a volume that included the updraft of a convective storm. The Doppler radar data do not provide the total picture, but they display more of the kinematic structure than can be obtained by other instruments.

The data obtained by the scanning Doppler radar illustrate both the utility and the limitations of single Doppler radar measurements. The radial velocity field from a single radar cannot yield the unambiguous three-dimensional wind fields that can be derived from dual-Doppler measurements; however, many features of the overall air motion in convective storms can be inferred from the radial velocity fields. This is especially true if, as in this case, the primary motion of the air entering and leaving the storm is in a vertical plane radial to the radar.

The second moment of the Doppler spectrum, obtained by a Doppler radar scanning the entire storm at low elevation angles, portrays regions of high shear and turbulence. The turbulence contribution can be isolated because shear can be inferred from the radial velocity fields. Measurement of the second moment fields and their evolution requires only a single radar. These data have not previously been fully utilized by radar meteorologists, but they can, in principle, provide a warning of dangerous turbulence or wind shear conditions and can aid in understanding how seed material or tracers will diffuse in a storm.

REFERENCES

Atlas, D., 1964: Advances in radar meteorology. *Advances in Geophysics*, Vol. 10, Academic Press, 318–478.

——, R. C. Srivastava and R. S. Sekhon, 1973: Doppler radar characteristics of precipitation at vertical incidence. *Rev. Geophys. Space Phys.*, **11**, 1–35.

Battan, L. J., 1974: Doppler radar observations of a hailstorm. *J. Appl. Meteor.*, **14**, 98–108.

Berger, T. and H. L. Groginsky, 1973: Estimation of the spectral moments of pulse trains. International Conf. Information Theory. Tel Aviv, Israel.

Browning, K. A., T. W. Harrold, A. J. Wyman and J. G. C. Beimers, 1968: Horizontal and vertical air motion and precipitation growth within a shower. *Quart. J. Roy. Meteor. Soc.*, **94**, 498–509.

Foote, G. B., and P. S. du Toit, 1969: Terminal velocity of raindrops aloft. *J. Appl. Meteor.*, **8**, 249–253.

Frisch, A. S., L. J. Miller and R. G. Strauch, 1974: Three-dimensional air motion measured in snow. *Geophys. Res. Lett.*, **1**, 86–89.

Joss, J., and A. Waldvogel, 1970: Raindrop size distribution and Doppler velocities. *Preprints 14th Radar Meteor. Conf.*, Tucson, Ariz.; Amer. Meteor., Soc., 153–156.

Lhermitte, R. M., 1963: Motions of scatterers and the variance of the mean intensity of weather radar signals. Sperry Rand Res. Center, 5RRC-RR-63-57, 25–28, Sudbury, Mass.

Miller, K. S., and M. M. Rochwarger, 1970: On estimating spectral moments in the presence of colored noise. *IEEE Trans. Inform. Theory*, **IT-16**, 303–309.

Nathanson, F. E., 1969: *Radar Design Principles; Signal Processing and the Environment.* McGraw-Hill, 626 pp.

Newton, C. W., 1963: Dynamics of severe convective storms. *Meteor. Monographs*, **5**, No. 27, 33–58.

Sirmans, D., and R. J. Doviak, 1973: Meteorological radar signal estimates. NOAA Tech. Memo. *ERL-NSSL-64*, U. S. Dept. of Commerce, Norman, Okla., 80 pp. [NTIS No. COM-73-11923/2AS].

Steiner, R., and R. H. Rhyne, 1962: Some measured characteristics of severe storm turbulence. National Severe Storms Project, Report No. 10, U. S. Dept. of Commerce [NTIS No. N62-16401].

Strauch, R. G., A. S. Frisch, and W. B. Sweezy, 1975: Doppler radar measurements of turbulence, shear, and dissipation rates in a convective storm. *Preprints 16th Radar Meteor. Conf.*, Houston, Tex., Amer. Meteor. Soc., 83–88.